Original Article

Landslide inventory and susceptibility assessment using multiple statistical approaches along the Karakoram highway, northern Pakistan

Mian Luqman HUSSAIN[1]* https://orcid.org/0000-0001-7452-7188; e-mail: mianluqman.geo@gmail.com

Muhammad SHAFIQUE[1] https://orcid.org/0000-0002-4063-6666; e-mail: shafique08@yahoo.com

Alam Sher BACHA[1] https://orcid.org/0000-0002-1467-7405; e-mail: mian.alamsher@gmail.com

CHEN Xiao-qing [2] https://orcid.org/0000-0002-1480-0266; e-mail: xqchen@imde.ac.cn

CHEN Hua-yong [2] https://orcid.org/0000-0003-4033-3339; e-mail: hychen@imde.ac.cn

Corresponding author

1 National Centre of Excellence in Geology, University of Peshawar, Peshawar 25130, Pakistan

2 Institute of Mountain Hazards and Environment, Chinese Academy of Sciences, Chengdu 610041, China

Abstract: China-Pakistan Economic Corridor (CPEC) is a framework of regional connectivity, which will not only benefit China and Pakistan but will have positive impact on Iran, Afghanistan, India, Central Asian Republic, and the region. The surrounding area in CPEC is prone to frequent disruption by geological hazards mainly landslides in northern Pakistan. Comprehensive landslide inventory and susceptibility assessment are rarely available to utilize for landslide mitigation strategies. This study aims to utilize the high-resolution satellite images to develop a comprehensive landslide inventory and subsequently develop landslide susceptibility maps using multiple techniques. The very high-resolution (VHR) satellite images are utilized to develop a landslide inventory using the visual image classification techniques, historic records and field observations. A total of 1632 landslides are mapped in the area. Four statistical models i.e., frequency ratio, artificial neural network, weights of evidence and logistic regression were used for landslide susceptibility modeling by comparing the landslide inventory with the topographic parameters, geological features, drainage and road network. The developed landslides susceptibility maps were verified using the area under curve (AUC) method. The prediction power of the model was assessed by the prediction rate curve. The success rate curves show 93%, 92.8%, 92.7% and 87.4% accuracy of susceptibility maps for frequency ratio, artificial neural network, weights of evidence and logistic regression, respectively. The developed landslide inventory and susceptibility maps can be used for land use planning and landslide mitigation strategies.

Keywords: Landslides; Inventory map; Susceptibility assessment; Northern Pakistan; CPEC

1 Introduction

The spatial likelihood of landslides is largely determined by local topography, geomorphology, geology, hydrology, landcover, tectonic features and human activities; and analyzed to evaluate the landslide susceptibility assessments (Reichenbach et al. 2018). Landslide susceptibility assessment models

often follow the assumption that the past and current conditions for landslides will remain consistent in the future (Zhou et al. 2018). Landslide susceptibility techniques can be qualitative or quantitative, whereas qualitative techniques inject subjectivity in descriptive susceptibility zonation and quantitative techniques estimate the probabilities of landslide occurrence in a susceptibility zone (Guzzetti et al. 1999; Reichenbach et al. 2018). Landslide susceptibility assessment initiates with the preparation of a comprehensive and realistic landslide inventory map, exhibiting the location, spatial extent, date of occurrence and type of the landslide (Guzzetti et al. 2012; Shafique et al. 2016). The developed landslide inventory maps are later compared with the predisposing geo-environmental factors including topography, geomorphology, geology, land cover, hydrology and other variables to evaluate the probability of terrain to cause a landslide and consequently assigned to the susceptibility level (Ilia and Tsangaratos 2016; Chen et al. 2017; Khan et al. 2018; Reichenbach et al. 2018; Riaz et al. 2018). Frequently applied landslide susceptibility models include the Analytical Hierarchy Model (Hung et al. 2015; Wu et al. 2016; Wang and Li 2017), Weight of evidence model (Neuhäuser et al. 2012; Ilia and Tsangaratos 2016;Razavizadeh et al. 2017), Frequency ratio (Wu et al. 2016; Wang and Li 2017; Khan et al. 2019) Artificial Neural Network (Yilmaz 2009; Pradhan and Lee 2010; Choi et al. 2012), Logistic Regression (Ozdemir and Altural 2013; Shahabi et al. 2014; Umar et al. 2014), Machine Learning Methods (Chen et al. 2016; Chen et al. 2017; Zhou et al. 2018), Certainty Factor (Wu et al. 2016) and Random Forest (Youssef et al. 2015; Kim et al. 2018; Park and Kim 2019). The majority of these studies utilize a single model for landslide susceptibility assessment, however, there is a growing trend of comparing the results from applying two or multiple models, and compare the derived landslide susceptibility maps (Reichenbach et al. 2018). Rossi et al. (2010) and Reichenbach et al. (2018) recommend applying multiple models for landslide susceptibility assessment and develop an "optimal" susceptibility zonation map to minimize the model uncertainty and its credibility to utilize for land use planning.

Mountainous terrains in northern Pakistan are frequently subjected to devastating land sliding driven by the rough terrain, the highest rate of tectonic uplift, active denudation, glaciation, climatic conditions,

climate change and human factors (Bishop et al. 1998; Hewitt 2009; Hewitt 2009; Bacha et al. 2018). Landslides in northern Pakistan are investigated by a range of researchers using field observations, geological records, tectonic features and historical records (Jones et al. 1983; Bishop et al. 1998; Derbyshire et al. 2001; Korup et al. 2007). (Ahmed and Rogers 2014) utilized geomorphic analysis of the hillshade map, to demarcate landslides with a length of > 500 m, which are subsequently used by Ahmed et al. (2014), for preliminary susceptibility assessment using expert-based weighted overall and fuzzy logic techniques. Calligaris et al. (2013) have used the topographic maps and field survey to map landslides in the Central Karakorum National Park (CKNP) and subsequently used to develop landslide susceptibility maps using the Analytical Hierarchy Process. This study aims to develop a comprehensive landslide inventory along the Karakorum Highway (KKH) as the major transportation corridor, using high-resolution satellite images supported with field observation and utilize it further to develop more realistic landslide susceptibility assessment using Weight of Evidence modeling, Frequency Ratio, Logistic Regression and Artificial Neural Network. The derived landslide susceptibility maps are compared and evaluated to determine the highly accurate landslide susceptibility map for the area.

2   Study Area

The study is conducted along the KKH, from Thakot to Chilas section in northern Pakistan (Fig. 1). Under the umbrella of the Belt and Road Initiative (BRI) of the Chinese government, the flagship segment is the China-Pakistan Economic Corridor (CPEC), aiming to link the Gwadar port in southern Pakistan with the Chinese city of Kashgar, through a network of roads and railways with a length of around 3000 km. The KKH in northern Pakistan is considered a critical section of the CPEC, however, it is prone to frequent disruption due to many geological and hydro-climatological hazards along the route. Among these, landslides are the most frequent and damaging to the highway, economic activities and human lives. Annual precipitation in the region varies from 127 mm to 1313 mm. Dominant landforms in the region are steep rock walls of hundreds of meters. Valleys in the region are filled with thick layers of
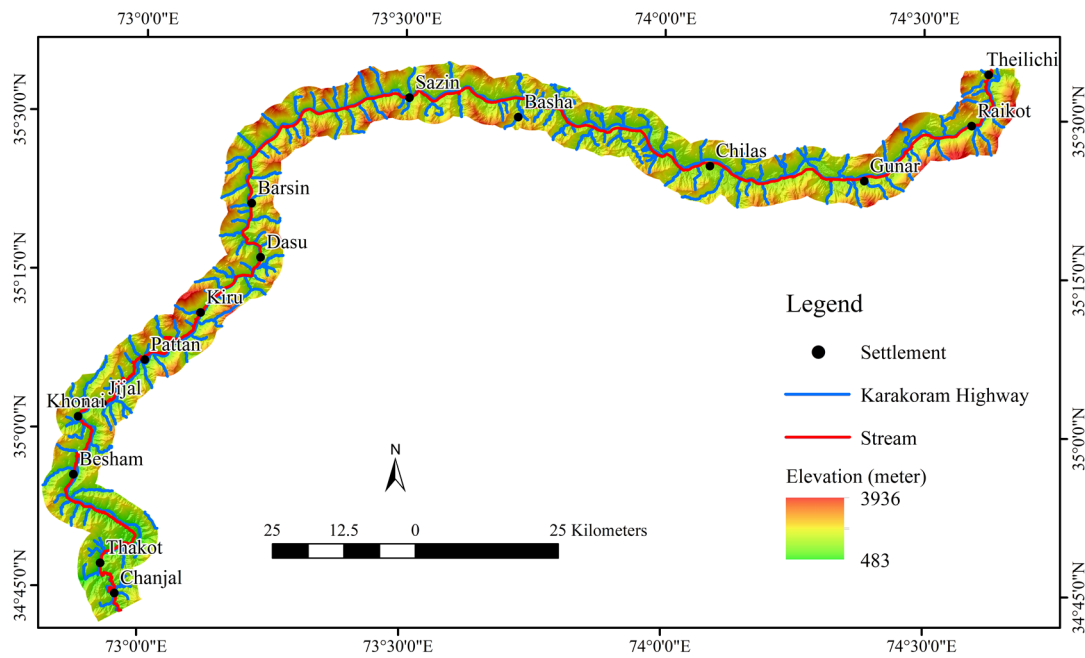
Fig.1 Location of the study area showing major towns along Karakoram Highway.

Table 1 Description of data used in the study

Data	Derived factors	Source
WorldView-2 Images (Resolution 0.46 m)	Landslide inventory Landcover Road	Digital globe
Documented records	Landslides inventory	Frontier Works Organization (FWO), published papers, police reports and revenue records
Shuttle Radar Topography Mission (SRTM) Digital Elevation Model (DEM) with 30-m resolution	Slope Aspect Distance to streams Curvature	(USGS 2017)
Geology Map at a scale of 1: 250,000	Geological Units	Geological Survey of Pakistan KKH Log, 2000

unconsolidated lacustrine, glacial and fluvial deposits. The presence of loose material on the steep slopes, valley floor and rugged topography support a high rate of erosion by the river Indus and its tributaries. Sediments of different origins (morainic, alluvial, lacustrine, debris-flow and aeolian) with a thickness of up to 100 m are unevenly distributed in the region (Owen 1988; Hewitt 1999). Most of these deposits are poorly consolidated and rarely cemented and hence are favorable for landslides in the form of debris flow and debris fall (Derbyshire et al. 2001). The combined impact of the high rate of erosion, rugged topography, active tectonics, anthropogenic factors makes this region one of the most prone to frequent and damaging landslides.

3   Materials and Methods

3.1 Landslide inventory

Visual interpretation of the acquired high-resolution WolrdView-2 Images at a spatial resolution of 0.46 m, supported with field knowledge is utilized for mapping the landslides. The WorldView-2 images were analyzed in 3D visualization by combining with the SRTM DEM, to precisely demarcate the landslides outline (Table 1). Spectral information, shape, roughness and color of the features on the images were used to demarcate the landslides (Chauhan et al. 2010).

The diagnostic shapes of various landslide types were also utilized to demarcate landslides and classified (Fig. 2) using Hunger et al. (2014) classification.

3.2 Causative factors

To evaluate the influence of the landslide causative factors on landslide distribution, a database
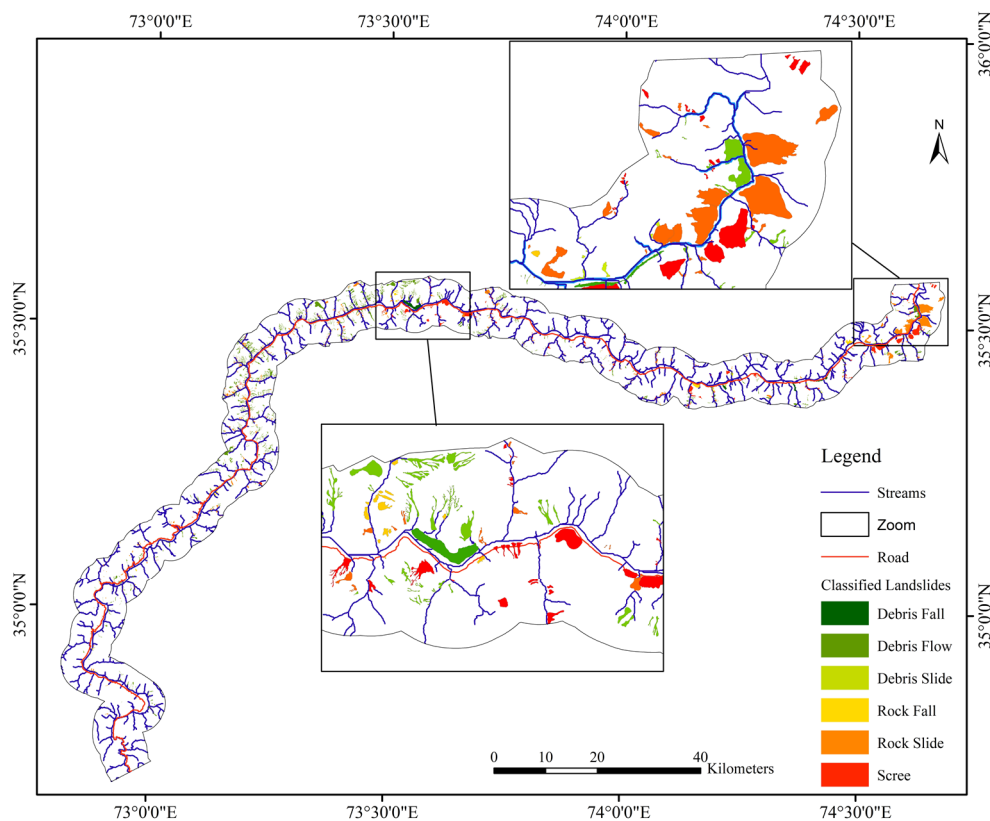
Fig.2 Spatial distribution of landslide types identified in the study area.

is developed comprising of topographic information and hydrological network derived from the DEM, geological information from the geological map and infrastructure from the utilized WorldView-2 image.

3.2.1 Topographic features

Topographic information of terrain elevation, terrain aspect, slope and curvature were computed from the Shuttle Radar Topography Mission (SRTM) DEM with a spatial resolution of 30 m.

3.2.2 Geology

Geological information of the area is derived from the Geological map of the area developed by the Geological Survey of Pakistan (GSP) with a scale of 1:250,000. Unfortunately, a large-scale geological map of the area was not available to capture the detailed geological information of the area. A total of nine geological formations were digitized (Fig. 3). Most of the historical large landslides in the region are located in close vicinity of the fault (Hewitt 2009). In the study area, the major faults include the Main Boundary Thrust (MBT) and the Main Mantle Thrust (MMT) system passes through the study area (Searle et al. 1999;Khan 2000). Faults in the region are mapped from the geological map of the area. Distance

from the faults was classified following Dou et al. (2015).

3.2.3 Roads and stream

The stream network of the area is computed from the SRTM DEM using the ArcHydro tools in ArcGIS. Six buffer zones of distance to stream were generated following Dou et al. (2015). Similarly, road construction in the study area involves excavation, land cutting and uncontrolled blasting that drive the slope instability and landslides (Yalcin et al. 2011). The road network of the area is extracted from the acquired WorldView-2 image for the area. Proximity to the road was classified into 6 different classes (< 10 m to > 200 m). All the selected causative factors were converted to raster maps with 30 m spatial resolution to utilize them for landslide susceptibility maps.

3.2.4 NDVI

The Normalized Difference Vegetation Index (NDVI) is the graphical representation of the distribution and intensity of the green vegetation and is usually computed from the remote sensing images. The NDVI layer is classified in to five class i.e. < 0.084, 0.084 - 0.221, 0.222 - 0.397, 0.398 - 0.577 and > 0.577 following (Nohani et al. 2019) (Fig. 3i).
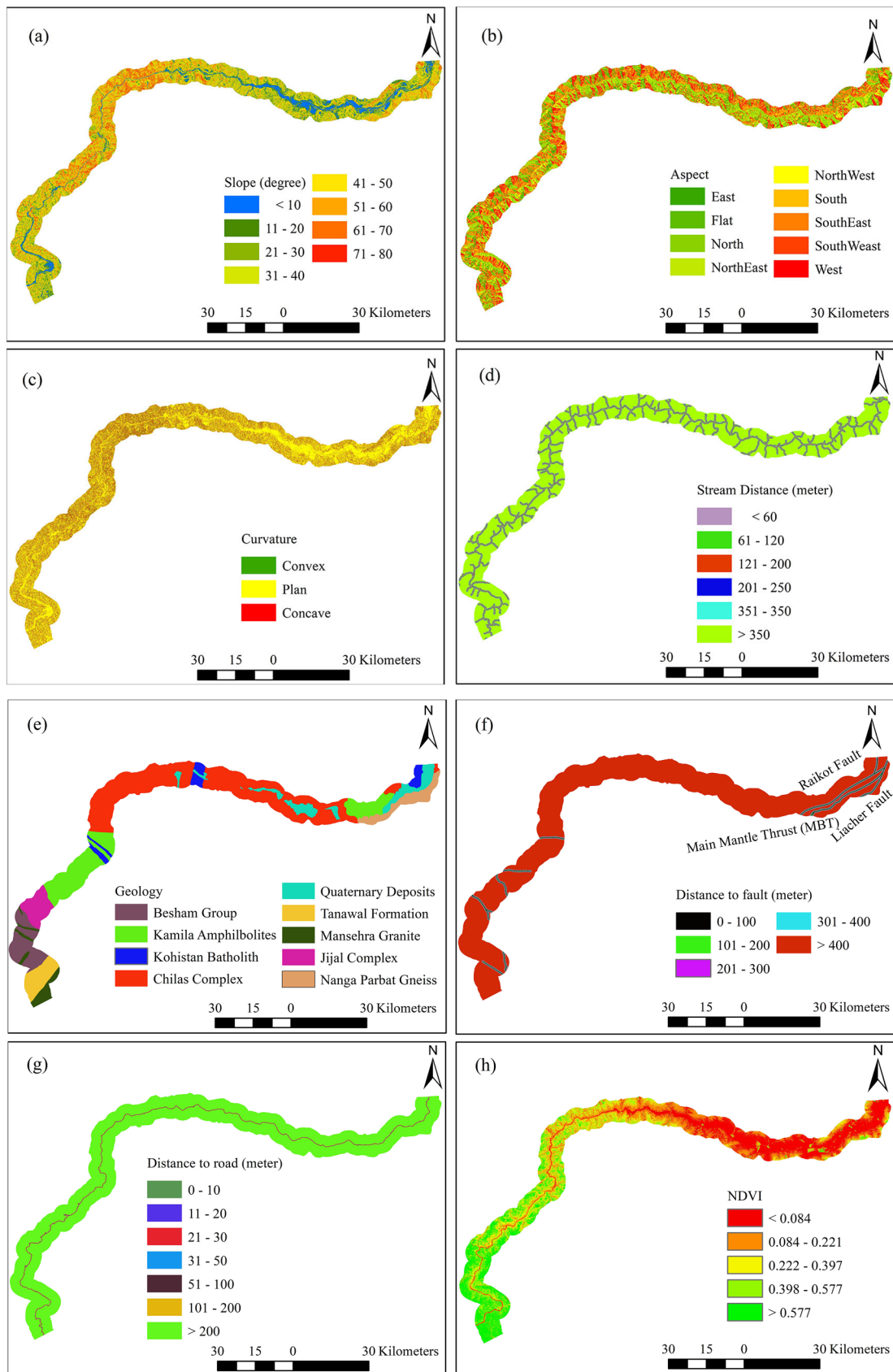
Fig. 3 Thematic layers of the selected causative factors used in the study to evaluate their impact on the spatial distribution of the landslides.

3.3 Description of methods

Landslide susceptibility assessment in the study area was implemented using the methods of Weight of Evidence Modelling (WofE), Frequency Ratio (FR), Logistic Regression (LR) and Artificial Neural Network (ANN). Using these methods, the influence of the selected causative factors on the landslide inventory is investigated to determine the susceptibility of the terrain to landslides.

3.3.1 Weights of evidence model

The Weight of Evidence (WofE) method is a quantitative technique for landslide susceptibility assessment. It is based on the Bayes theorem and evaluates the relative significance of each class of the independent variables on the dependent variable (Bonham-Carter 1994). The theoretical background and mathematical algorithms of the WofE are explained by Bonham-Carter et al. (1988), Bonham-Carter et al. (1989) and Bonham-Carter et al. (1994).

3.3.2 Artificial Neural Network (ANN)

A neural network is the model of argumentation based on the human brain comprising of interconnected nerve cells or neurons (Negnevitsky 2011). The ANN is repeatedly utilized to evaluate landslide susceptibility assessment by analyzing the landslide inventory and causative factors (Lee et al. 2001; Caniani et al. 2008; Aditian et al. 2018; Valencia Ortiz and Martínez-Graña 2018). The multi-layer perceptron (MLP) neural network explained by (David and James 1987) is one of the most extensively used ANN techniques (Pijanowski et al. 2002). The MLP network consists of three layers i.e. input, hidden, and output layers and can identify associations that are non-linear (Pijanowski et al. 2002). The correlations between the variables and neural network equations were established in ArcGIS 10.5. Subsequently, the landslides and non-landslides point data are partitioned into "training data" and "test data". The 1300 landslides and 1300 non-landslide points were selected for training the ANN. Similarly, 331 landslides and 331 non-landslide points were used for the prediction testing. The popular ANN model used in prediction tasks is the Multi-Layer Perceptron (MLP) with a feed-forward back-error propagation (BP) type of learning algorithm. A three-layer feed forward MLP learning algorithm was trained, which consists of one input layer, two hidden layer, and one output layer. After the final weight calculation, GIS-based weighted linear combination was used in the ArcGIS using the Eq. 1.

$$LS = \sum_{i=1}^{n} f_{wi} \times s_{ij} \qquad (1)$$

Where LS is the final ANN weights, f_{wi} is the importance of the landslide causative factor i, and s_{ij} is the rescaled weight for category j of factor i. The LSI map was subsequently classified into five classes based on the "Natural Breaks" method.

3.3.3 Logistic Regression

Logistic regression is frequently applied for landslides susceptibility assessment, considering the landslide inventory as the dependent variables and the selected causative factors as the independent variables (Meng et al. 2016; Lucas and Sven 2017; Aditian et al. 2018; Schlögel et al. 2018). The total number of landslide pixels and an equal number of randomly selected cells from non-landslide areas and were divided into training (70 %) and validation (30%) dataset. Therefore, the developed landslide inventory as the dependent variable and the selected landslide causative factors as the independent variables were converted to ASCII format and analyzed using logistic regression modeling in the statistical package of SPSS.

3.3.4 Frequency Ratio

The frequency ratio is based on the relationship between the spatial distribution of landslides and each conditioning parameter. The frequency ratio (FR) method for landslide susceptibility assessment aims to quantify the association between the mapped landslide inventory and selected causative factors and is frequently applied for landslide susceptibility mapping (Yilmaz 2009;Reis et al. 2012;Umar et al. 2014;Chen et al. 2016;Wu et al. 2016;WangLi 2017;Khan et al. 2018). FR is the ratio of the area where the landslides occur to the total area so that the value of 1 is an average value. If the value is greater than 1, reflects that the percentage of the landslide is higher than the area and indicates a higher correlation, whereas values lower than 1 indicate a lower correlation (Akgun et al. 2007).

3.4 LSI maps, validation and comparison

The Landslide Susceptibility Index (LSI) maps derived from the selected models were compared and validated to evaluate the more accurate landslide susceptibility map. The derived LSI maps were

Table 2 Mapped landslide types, min/max area and flow length in the study area

Landslide Types	No.	Landslide (%)	Area (km²)				Run out distance (m)		Slope (°)		Elevation (m)	
			Min	Max	Average	Total	Min	Max	Min	Max	Min	Max
Rock fall	101	6.19	0.010	0.668	0.040	29.78	76.02	1560.03	14.7	67.2	594	2097
Debris fall	13	0.80	0.001	1.940	0.356	4.63	49.04	2286.01	7.1	50.2	1126	1615
Scree	146	8.95	0.526	1.882	0.104	15.16	107.90	1674.02	16.6	58.6	1087	2489
Rockslide	518	31.74	0.031	3.523	0.057	29.78	16.60	4536.02	3.5	70.3	630	2886
Debris slide	28	1.72	0.070	0.122	0.034	0.96	67.20	3009.1	7.9	61.0	586	1766
Debris flow	826	50.61	1.138	0.048		39.46	6.20	3421.4	16.3	66.9	654	3028
Total	1632					119.80						

validated through Success Rate Curve (SRC) and R-index (Shahabi et al. 2014). The success rate curve was calculated by crossing the validation landslide modeling data set with the LSI map. From the success rate curve area under the curve (AUC) was calculated. To acquire both values, the LSI values were sorted into descending order. Then the ordered grid values of the LSI were categorized into 100 classes' with 1% cumulative intervals, for which the cumulative percentage of landslide occurrence in the classes was calculated to get the AUC. Landslide susceptibility maps generated in this study were also validated following Shahabi et al. (2014) relative landslide density method (R-index).

4 Results

4.1 Landslide inventory

A total of 1632 landslides were identified and mapped with a total area of 119.77 km². The smallest landslide is identified with an area of 0.001 km², while the largest landslide is identified with an area of 3.52 km². 35 landslides are exceeding 1 km² area, while 60% of the landslides have an area between 400 to 500 m². Among the mapped landslides, 50.61% of the landslides are debris flows. Rockslides are the second most frequently occurring phenomenon in the area with a share of 31.74% area. The majority of the historical large rockslides with the potential of blocking the river Indus and leading to natural dams occurred in the Nanga Parbat Haramosh Massif (NPHM). The largest mapped rockslide in the area has an area of 3.523 km². Scree slopes are identified and distinguished from the talus based on fractured materials (Fig. 4). There are 146 scree slopes in the study area with a share of 8.95% among the total mapped landslides.

We have mapped 101 rockfalls in the study area. Most of the rockfalls were present along with the MBT and Raikot fault system. Rocks fall covers 29.78 km² of the total landslide area. Debris fall and debris slides were 13 and 28 in numbers respectively (Table 2).

4.2 Relationship between landslides occurrences and causative factors

4.2.1 Weights of Evidence and Frequency Ratio

Slope gradient: The distribution of several pixels and their percentages in each slope class. In the slope gradient layer highest positive weight (W^f) value of 0.59 and 0.85 is calculated for 31°- 40° to >70° classes respectively. The lowest and negative weight is observed for the slope gradient classes of 0 -10° (-1.40) and 10-20° (-0.19). The 60° and >70° slope gradient show higher frequency ratios of 1.09 and 1.94, respectively.

Slope aspect: It is observed that the northeast aspect shows the lowest and negative correlation with the W^f value of -0.48. The highest frequency ratio values were calculated for southwest and west-facing slopes. The Northeast facing slope shows the lowest frequency ratio of 0.80.

Curvature: Curvature classes are comprised of concave, flat and convex classes (Table 3). A negative correlation was observed for flat and convex curvature with the W^f value of -0.07 and -0.17, respectively. The concave curvature class shows a positive correlation with the W^f value of 0.19 and the highest frequency ratio value of 1.02.

NDVI: The NDVI class of < 0.084 is showing the highest weight (W^f) and frequency ratio of 1.21 and 1.89 respectively and indicating a positive correlation between landslides and causative factors (Table 3). The negative and lowest W^f value of -2.99 and frequency ratio value of 0.02 was calculated for class > 0.577 and thus less susceptible to landslide occurrences.

Distance to roads: Landslide susceptibility is decreasing as the distance from the road increases.
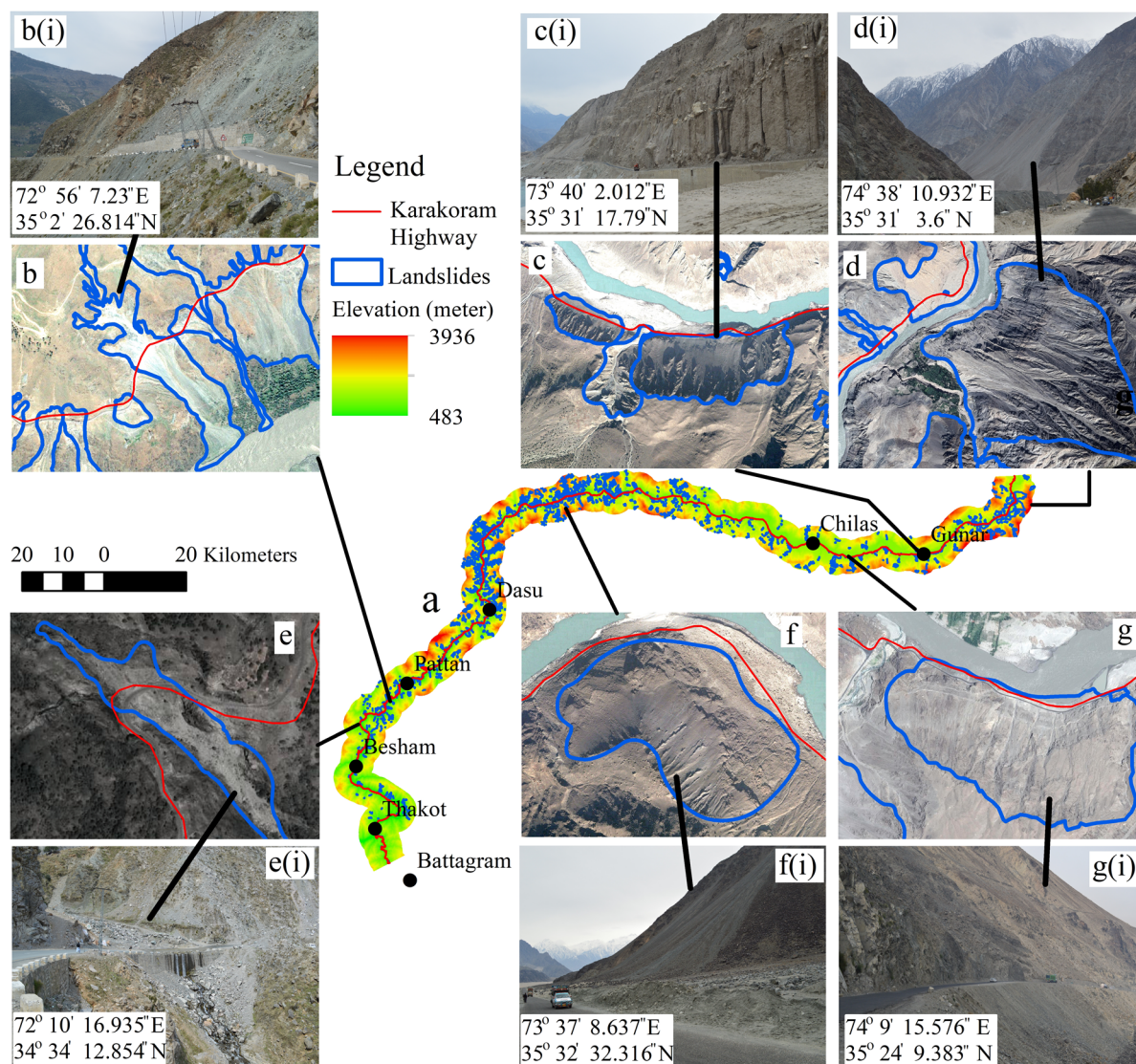
Fig. 4 (a) shows landslide inventory of the study area on SRTM DEM, (b), (c), (d), (e), (f) and (g) are showing zoom location of landslide polygons overlaying on the WorldView-2 image. b (i) is a picture of rockfall along the KKH road near Jijal, c (i) is showing debris fall near Gunar, d (i) is showing rockslide, e(i) is showing debris flow near Dubair, f(i) is showing scree slope and g(i) is showing debris slide near Chilas.

The calculated weight for distance to road class of 11-20 m is highest with a positive W^f value of 1.20 and the highest frequency ratio of 1.21, while the lowest W^f value of -0.83 and lowest frequency ratio of 0.99 for distance to road class of >200 m (Table 3).

Distance to faults: The highest W^f values (1.06, 1.02) and frequency ratio (1.75, 1.73) were calculated for the distance to fault class of < 100 and 101-200 m. Up to 400 m distance to the fault class, the calculated weight is positive, while > 400 m the calculated W^f value is 0.43 and the frequency ratio is the lowest (0.96) (Table 3). The results show that the landslide area is decreasing with increasing distance from the faults.

Distance to streams: It is evident from Table 3 that the highest percentage (79.3%) of landslides are located in > 350 m class in distance to streams, with 0.48 W^f value. It is observed that the highest W^f values are calculated for the 251-350 m class in the distance to the stream layer.

Geology: The highest values of 1.08 (W^f) and 2.67 (frequency ratio) are calculated for the Quaternary Deposits class followed by Nanga Parbat Gneiss (Table 3). The lowest W^f values (-2.25) and the lowest frequency ratio value (0.06) are observed for the Mansehra Granite and Tanawal Formation.

Table 3 Descriptive statistics of the influence of causative factors classes on the landslides using the weight of evidence modeling and frequency ratio methods.

Causative Factors	Class	Class Pixels	Class Pixel (%)	Landslide Pixels	Landslide Pixel (%)	Frequency Ratio	(Wf)
Slope (°)	0-10	238797	8.5	2726	2.3	0.33	-1.40
	11-20	310702	11.1	7705	6.5	0.52	-0.19
	21-30	430329	15.3	15445	13.1	1.01	0.51
	31-40	540138	19.2	24387	20.7	1.05	0.59
	41-50	538950	19.2	27322	23.2	0.93	0.35
	51-60	413754	14.7	21294	18.1	0.94	0.36
	61-70	242817	8.7	13035	11.1	1.09	0.64
	>70°	90692	3.2	5743	4.9	1.94	0.85
Aspect	Flat	2649	0.1	23	0.0	0.00	0.00
	North	382390	13.6	12509	10.6	0.90	-0.29
	Northeast	350349	12.5	9687	8.2	0.80	-0.48
	East	345670	12.3	11236	9.5	0.93	-0.30
	Southeast	354341	12.6	18231	15.5	0.99	0.19
	South	337523	12.0	17050	14.5	0.92	0.22
	Southwest	313560	11.2	15650	13.3	1.12	0.21
	West	353114	12.6	17348	14.7	1.24	0.25
	Northwest	366583	13.1	15923	13.5	1.02	0.04
Curvature	Concave	287290	10.2	16464	14.0	1.02	0.19
	Flat	1866080	66.5	77452	65.8	1.04	-0.07
	Convex	652809	23.3	23741	20.2	0.81	-0.17
NDVI	< 0.084	800385	28.5	145502	53.8	1.89	1.20
	0.084 - 0.221	620613	22.1	89395	33.0	1.50	0.62
	0.222 - 0.397	471680	16.8	27343	10.1	0.60	-0.63
	0.398 - 0.577	443566	15.8	7266	2.7	0.17	-2.01
	> 0.577	473372	16.8	1139	0.4	0.02	-2.99
Distance to road	< 10	7750	0.3	896	0.8	1.10	1.10
	11-20	7828	0.3	984	0.8	1.21	1.20
	21-30	7652	0.3	942	0.8	1.16	1.17
	31-50	15576	0.6	1771	1.5	1.13	1.09
	51-100	38057	1.4	3579	3.0	1.08	0.88
	101-200	74578	2.7	4826	4.1	1.02	0.47
	>200	2654738	94.6	104659	89.0	0.99	-0.83
Distance to fault	<100	41352	1.5	4516	3.8	1.75	1.06
	101-200	40630	1.4	4319	3.7	1.73	1.02
	201-300	39974	1.4	3776	3.2	1.69	0.89
	301-400	39510	1.4	3491	3.0	1.76	0.81
	>400	2644713	94.2	101555	86.3	0.96	0.43
Distance to stream	<60	73404	2.6	2000	1.7	0.57	0.26
	61-120	67581	2.4	3310	2.8	0.96	0.17
	121-200	92726	3.3	6548	5.6	1.17	0.58
	201-250	53440	1.9	4168	3.5	1.29	0.68
	251-350	110809	3.9	8306	7.1	1.33	0.75
	>350	2408219	85.8	93325	79.3	0.97	0.48
Geology	Besham Group	225087	8.0	1519	1.3	0.07	-1.94
	Kamila Amphilbolites	507005	18.1	12705	10.8	0.59	0.62
	Kohistan Batholith	121236	4.3	4729	4.0	1.23	0.22
	Chilas Complex	1183155	42.2	57461	48.8	1.29	0.28
	Quaternary Deposits	221603	7.9	22453	19.1	2.67	1.08
	Tanawal Formation	149858	5.3	826	0.7	0.06	-2.12
	Mansehra Granite	96007	3.4	453	0.4	0.06	-2.25
	Jijal Complex	148403	5.3	3130	2.7	0.25	0.14
	Nanga Parbat Gneiss	153825	5.5	14381	12.2	1.60	0.93

Note: W^f = Weights of Evidence final weights.

4.2.2 Logistic Regression

The influence of selected causative factors on landslide distribution in the area use logistic regression. The "significance probability value" was less than 0.05 against all variables except aspect, distance to fault, curvature and lithology. The rest of the five causative factors are having a significant effect on landslide occurrences. The regression

coefficients calculated for each causative factor were expressed as shown in Eq. 2 to develop the LSI map.

Ln (-3.291) + (Slope*0.06) + (Aspect* -0.006) + (Curvature*-0.059) + (NDVI*-0.743) + (Distance to road *-0.000) + (Distance to fault *0.002) + (Distance to stream*0.000) + (Lithology*0.006) (2)

The variables with coefficients having a significant probability of less than 0.05 were accepted as influential variables. Chi-square determines the difference between likelihood and null hypothesis, in which all the coefficient values are set to 0, which measures the improvement in fit based independent variables in the regression. Significant probability values of 0 show that slope, NDVI, distance to road and distance to stream are more significant than the distance to fault and lithology with values 0.008 and 0.007, respectively. Table 4, shows a summary of the overall statistics of logistic regression in the study area.

4.2.3 Artificial Neural Network

According to the results of the partitioning of ANN connection weights, the factors of terrain slope, NDVI, distance to road and distance to stream, with importance values of 0.16 each reflecting their significant influence on landslides. Distance to fault and lithology got the importance values of 0.09 and 0.09, respectively. On the contrary, aspect and curvature have the lowest importance with values 0.06 and 0.08, respectively (Table 5).

4.3 Landslide Susceptibility Index map (LSI)

After calculating the final weight for each of the landslide causative factors the resultant weights calculated using WofE, FR, ANN and LR (Table 3, 4 and 5) were summed to develop the Landslide Susceptibility Index (LSI) maps. The LSI maps were classified into four classes (low, moderate, high and very high) using the natural breaks method following Das et al. (2010) to develop a landslide susceptibility zonation map (Figs. 5 and 6).

4.4 Accuracy assessment of susceptibility maps and models prediction

The Landslide Susceptibility Index (LSI) maps were validated using the success rate curve following Dou et al. (2015) (Fig. 7a). From the qualitative analysis of the AUC of success rates curve, an accuracy of 92.8 % for ANN, 92.7% for WofE, 87.4%

Table 4 Coefficients of the logistic regression model

Causative Factors	Logistic coefficient	Standard error	Significance probability
Slope	0.060	0.003	0.000
Aspect	-0.006	0.015	0.675
Curvature	-0.059	0.091	0.518
NDVI	-0.743	0.063	0.000
Distance to road	0.000	0.000	0.000
Distance to fault	0.002	0.000	0.008
Distance to stream	0.000	0.000	0.000
Lithology	0.006	0.020	0.007
Constant	-3.291	0.343	0.000

Table 5 Derived Artificial Neural Network (ANN) weights for utilized causative factors

Causative factors	Importance	Normalized importance
Slope (°)	0.16	98.80%
Aspect	0.08	50.90%
Curvature	0.06	36.80%
NDVI	0.16	100.00%
Distance to road	0.16	99.10%
Distance to fault	0.09	53.70%
Distance to stream	0.16	96.70%
Lithology	0.09	58.30%

for LR and 93.1% for the FR model is achieved. From the prediction rate curve (Fig. 7b), the prediction value of 90.1%, 86.4%, 85.6% and 88.3% are calculated for ANN, WofE, LR and FR, respectively. The R-index sample datasets for a very high hazard class in FR, WofE, ANN and LR maps are 128.2%, 192.8%, 179.4% and 126.2%, respectively. The R-index validation is given in Table 6.

4.5 Validation and comparison of models for landslide susceptibility

Landslide distribution in susceptibility classes developed using all four methods were compared. Li increases from low to very high susceptibility classes in all methods (Table 7). Therefore, all the methods used for susceptibility mapping produced acceptable results. However, the highest accuracy was obtained from ANN (81%) followed by LR (78%) method comparable to FR (77%) and WofE (72%) method.

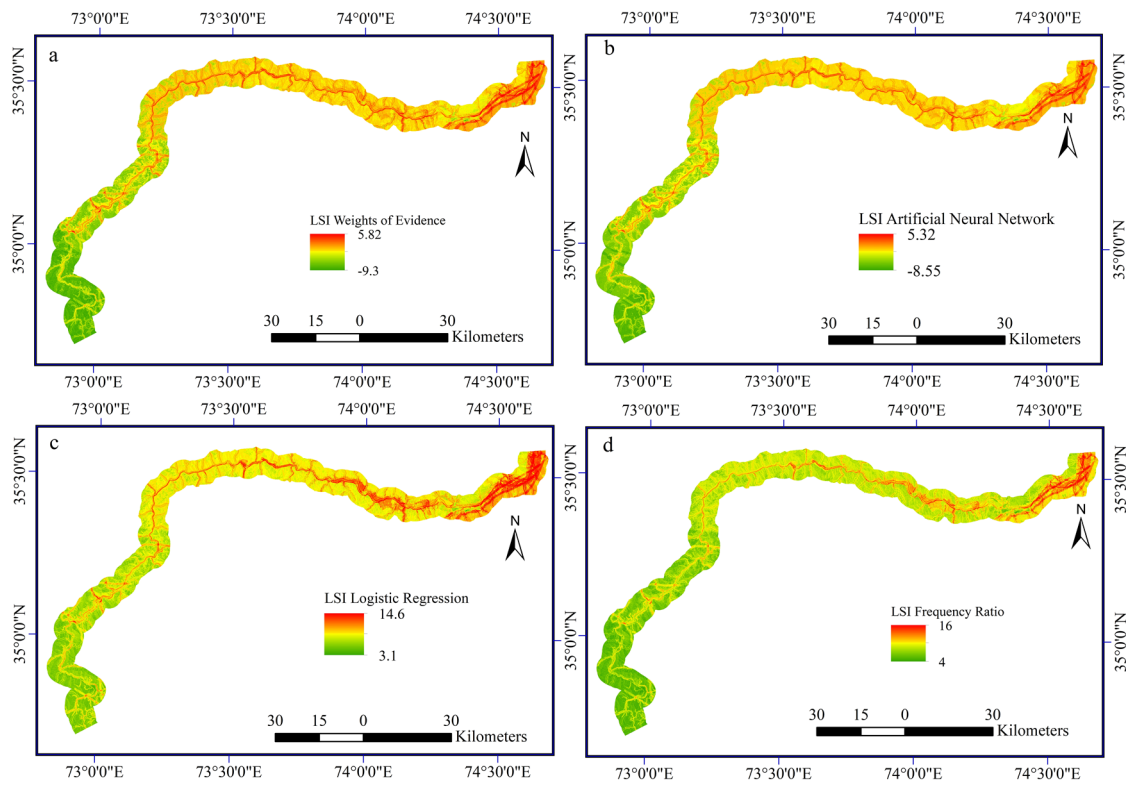## 5 Discussion

This study developed comprehensive and

Fig. 5 Landslide susceptibility index maps developed using the (a) Weight of evidence modeling (b) Artificial neural network (c) Logistic regression and (d) Frequency ratio.
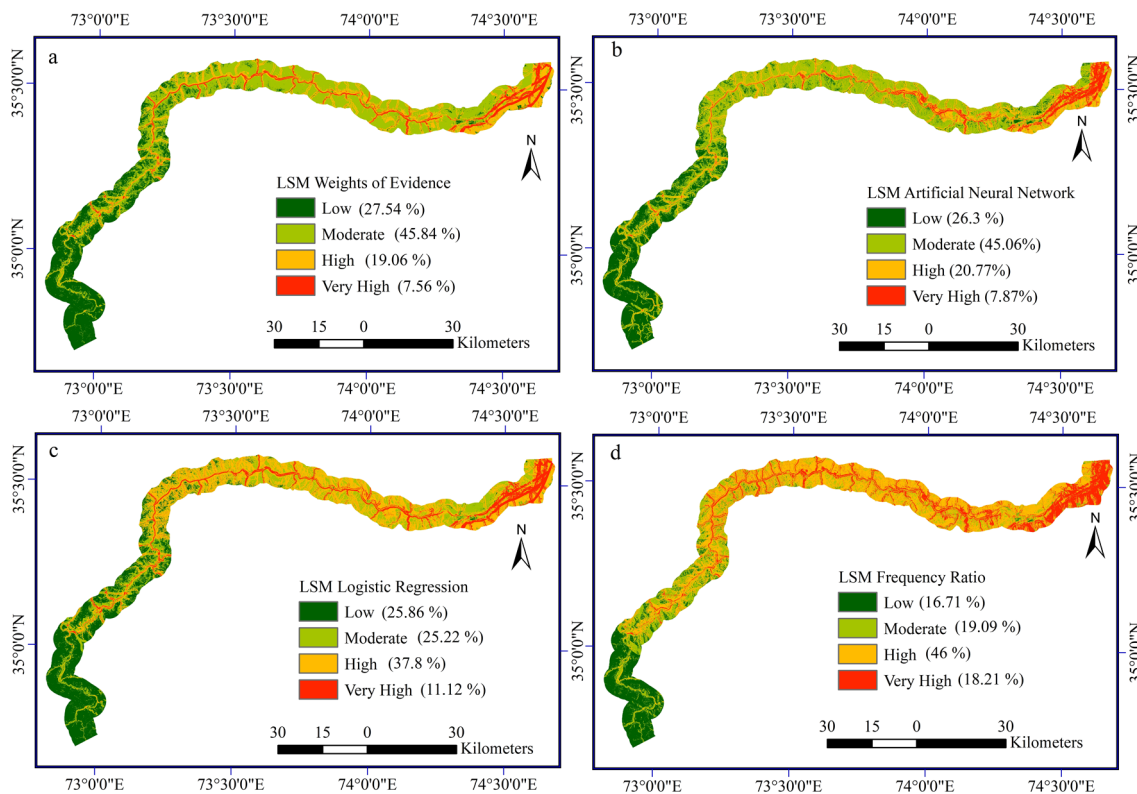

Fig. 6 Landslide susceptibility index maps were classified in different susceptibility classes using natural break (a) Weight of evidence modeling (b) Artificial neural network (c) Logistic regression and (d) Frequency ratio.
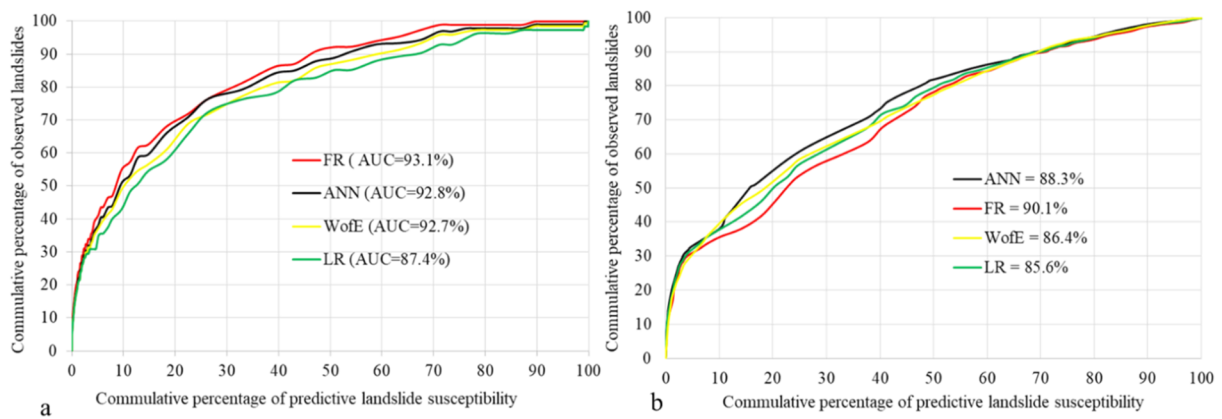
Fig. 7 (a) Success rate curves of the model, showing the cumulated number of landslides captured by the susceptibility map (b) Prediction rate curves of the model, showing the cumulated number of landslides captured by the susceptibility map.

Table 6 Validation (R-index) of Frequency Ratio (FR), Weights of Evidence (WofE), Artificial Neural Network (ANN) and Logistic Regression (LR) methods.

Validation Models	Susceptibility class	Number of Pixels	Area percentage	No of landslides	Landslide %	R-Index
FR	Low	737527	26.3	77	4.6	17.5
	Moderate	1263275	45.06	771	46.1	102.2
	High	582264	20.77	657	39.2	189.0
	Very High	220708	7.87	169	10.1	128.2
WofE	Low	724942	25.86	59	3.5	13.6
	Moderate	707170	25.22	334	20.0	79.1
	High	1059781	37.8	922	55.1	145.7
	Very High	311881	11.12	359	21.4	192.8
ANN	Low	772022	27.54	73	4.4	15.8
	Moderate	1285351	45.84	737	44.0	96.0
	High	534494	19.06	637	38.1	199.6
	Very High	211907	7.56	227	13.6	179.4
LR	Low	701411	25.02	63	3.8	15.0
	Moderate	1353458	48.27	831	49.6	102.8
	High	533952	19.04	618	36.9	193.9
	Very High	214953	7.67	162	9.7	126.2

detailed landslide inventory for the study area. The number of landslides varies from other studies on the area including Ahmed et al. (2014), Ali et al. (2019), Bacha et al. (2018) and Hewitt (2009), which can be attributed to the difference in the extent of the study area, methodology and utilized satellite images for mapping the landslides. In the area, scree is usually observed on the steep slopes where the eroded debris and detached rock from upstream are deposited on the slopes. Scree slopes are unconsolidated debris lying on steep slopes and often result in debris flows during the rainy season. Hewitt (2009) and Ali et al. (2019) also confirmed debris flow activity in these historical large rock slide materials.

Loose debris of the historical landslides are deposited at the slope toe, which is often reactivated in the form of multiple debris flows during the rainy season. Given the high and steep relief, these debris flows travel long distances and often damaged the KKH. At many locations, these loose materials of the historical landslides are excavated vertically for the KKH construction (Fig. 8).

Among the selected landslide causative factors the terrain slope, distance to road, lithology and distance to a fault have a significant influence in the spatial arrangements of landslides, which is also observed by Ali et al. (2019), Bacha et al. (2018) and Khan et al. (2018). Among the geological units, the Quaternary Deposits and Chilas Complex are most susceptible to landslides. The Chilas Complex has 42.2% spatial coverage in the study area and hosting the majority of the landslides. It was observed that

lithologies of the Nanga Parbat Gneiss and Chilas Complex are highly deformed and fractured due to the presence of active faults (i.e. MMT and Raikot faults), also endorsed by Ahmed et al. (2014), Chen et al. (2011), Hewitt (2009) and Ali et al. (2019). Landslides are mostly concentrated within a distance of 400 ms from the fault. Hewitt (2009) reported that the high rate of landslide initiation in the Raikot area is related to seismically active fault systems. Ahmed et al. (2014) reported that seismic activities along with the MMT and Riakot fault systems, are the major trigger for the initiation of landslides. The slope angle of >30° shows

a positive correlation with the landslide's occurrences. A total of 20.7% of the landslides were observed in the slope class of 31°-40° and 23.2% in 41°-50°. Among the slope gradient classes, the highest value of WofE (0.85) and FR (1.94) values are calculated for >70° class. A similar observation of landslide occurrences was also investigated by Neuhauser et al. (2012). Bacha et al. (2018) have also reported higher weights for 30° to 60° slope along the KKH. Among the terrain aspects, north, northeast, east and northwest got the lowest weights shows negative correlation which is an agreement with Bacha et al. (2018). The

Table 7 Comparison of the precision information obtained from crossing each of the susceptibility maps with the map of landslides distribution following Shahabi et al. (2014).

Method	Susceptibility classes	A_i (km²)	S_i (km²)	Density of slide in any class	Density of slide in whole map	$n(S_i/A_i)$	Susceptibility class (%)	K_s (km²)	S (km²)	P
FR	Low	663.8	12.2	0.02			26.3			
	Moderate	1136.9	103.0	0.09	0.097	0.11	45.1	188	243.6	0.77
	High	524.0	72.8	0.14			20.8			
	Very High	198.6	55.6	0.28			7.9			
WofE	Low	652.4	3.1	0			25.9			
	Moderate	636.5	56.4	0.09	0.097	0.11	25.2	175.9	243.6	0.72
	High	953.8	116.4	0.12			37.8			
	Very High	280.7	67.7	0.24			11.1			
ANN	Low	694.8	4.2	0.01			27.5			
	Moderate	1156.8	116.0	0.10	0.097	0.11	45.8	196.7	243.6	0.81
	High	481.0	76.5	0.16			19.1			
	Very High	190.7	46.8	0.25			7.6			
LR	Low	631.3	8.7	0.01			25.0			
	Moderate	1218.1	112.7	0.09	0.097	0.11	48.3	188.7	243.6	0.78
	High	480.6	67.4	0.14			19.0			
	Very High	193.5	54.9	0.28			7.7			

Note: S_i= slide area in each susceptibility zone, A_i= area of each zone, n = number of susceptibility classes, K_s = area of slide zone in upper moderate susceptibility level, S = area of landslide in the region, P = precision of the predicted results.
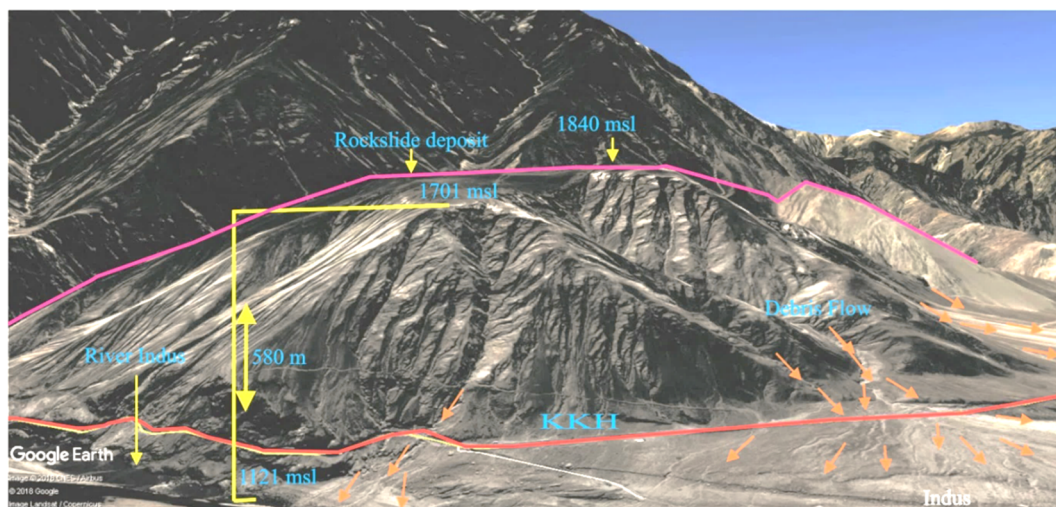

Fig.8 3D visualization of Google earth image showing remnants of a historic rockslide that is now a source of debris flows during rainfall.

highest value of W^{T} (0.25) and FR (1.24) is derived for the west-facing slope. The slopes facing southeast to the southwest are more susceptible to landslides and hosts 36% area of the total landslide area. Landslides distribution was intensified within 100-200 m distance to roads and >250 m to the streams.

Accuracy assessment of susceptibility maps shows that the FR model results are more accurate than other models followed by the ANN model. Similarly, 92.8% success rate curves areare calculated for the ANN model respectively (Fig. 7a). LR and WofE show 87.4% and 92.7 % validation calculated from the success rate curve. The prediction power of the FR model is highly comparable to other models calculated from the prediction rate curve, followed by ANN (88%), LR (85.6%) and WofE (86.4%). The prediction accuracy obtained for FR, WofE, ANN and LR in this study are almost similar to previous studies such as (Polykretis and Chalkias 2018) used WofE, LR and ANN models for their landslide susceptibility study and obtained a prediction accuracy of 84%, 83% and 78%, respectively. (Ozdemir and Altural 2013) , conducted a landslide susceptibility comparative study for Sultan Mountains, Turkey, using WofE, FR and LR models and their results show an accuracy of 93%, 97% and 95 %, respectively.

6   Conclusion

This study presents a landslide inventory and susceptibility in 8 km buffer along the KKH from Thakot to the Thelichi area in northern Pakistan. Visual Interpretation of WorldView-2 remote sensing image with field verification and road maintenance records leads to the mapping of 1632 landslides with a total area of 119.8 km². Among the mapped landslides, 50% are debris flows and 31.7% are rockslides. Landslide inventory is correlated with causative factors using WofE, ANN, FR and LR statistical models for development of susceptibility map to demarcate the region vulnerable to landslides in the future. The purpose of these four frequently used models for landslide studies was to assess the accuracy and suitability of the models for landslide susceptibility mapping in the study area. From the comparison of model results, it has been found that FR model is better followed by ANN model comparable to WofE and LR for landslide susceptibility mapping in the study area. It has been observed that terrain slope, geology, distance to roads and distance to fault are a major influence on the landslide occurrences in the study area. The results from this study can be used for landslide hazard and risk assessment in the study area and hence can play a role in mitigation strategies to cope with landslide hazards.

References

Aditian A, Kubota T, Shinohara Y (2018) Comparison of GIS-based landslide susceptibility models using frequency ratio, logistic regression, and artificial neural network in a tertiary region of Ambon, Indonesia. Geomorphology 318: 101-111. https://doi.org/10.1016/j.geomorph.2018.06.006

Ahmed MF, Rogers J (2014) First-approximation landslide inventory maps for Northern Pakistan, using Aster DEM data and geomorphic indicators. Environ Eng Geosci 20: 67-83. https://doi.org/10.2113/gseegeosci.20.1.67

Ahmed MF, Rogers JD, Ismail EH (2014) A regional level preliminary landslide susceptibility study of the upper Indus river basin. Eur J Remote Sens 47(1): 343-373. https://doi.org/10.5721/EuJRS20144721

Akgun A, Dag S, Bulut F (2007) Landslide susceptibility mapping for a landslide-prone area (Findikli, NE of Turkey) by likelihood-frequency ratio and weighted linear combination models. Eng Geol 54: 1127-1143.

Ali S, Biermanns P, Haider R, et al. (2019) Landslide susceptibility mapping by using a geographic information system (GIS) along the China–Pakistan Economic Corridor (Karakoram Highway), Pakistan. Nat Hazards Earth Syst Sci 19(5): 999-1022.

Bacha AS, Shafique M, van der Werff H (2018) Landslide inventory and susceptibility modelling using geospatial tools, in Hunza-Nagar valley, northern Pakistan. J Mt Sci 15(6): 1354-1370. https://doi.org/10.1007/s11629-017-4697-0

Bishop MP, Shroder Jr JF, Hickman BL, et al. (1998) Scale-dependent analysis of satellite imagery for characterization of glacier surfaces in the Karakoram Himalaya. Geomorphology 21(3–4): 217-232. http://doi.org/10.1016/S0169-555X(97)00061-5

Bonham-Carter GF (1994) Geographic Information Systems for Geoscientists, Modeling with GIS, Oxford: Pergamon Press.

Bonham-Carter GF, Agterberg FP, Wright DF (1988) Integration of geological datasets for gold exploration in Nova Scotia. Photogramm Eng Remote Sensing 54: 1585–1592.

Bonham-Carter GF, Agterberg FP, Wright DF (1989) Weights of

evidence modelling: a new approach to mapping mineral potential. Statistical Applications in the Earth Science,. GDC Paper 9 (89): 171–183.

Calligaris C, Poretti G, Tariq S, et al. (2013) First steps towards a landslide inventory map of the Central Karakoram National Park. Eur J Remote Sens 46(1): 272-287. https://doi.org/10.5721/EuJRS20134615

Caniani D, Pascale S, Sdao F, et al. (2008) Neural networks and landslide susceptibility: a case study of the urban area of Potenza. Nat Hazards 45(1): 55-72. https://doi.org/10.1007/s11069-007-9169-3

Chauhan S, Sharma M, Arora MK (2010) Landslide susceptibility zonation of the Chamoli region, Garhwal Himalayas, using logistic regression model. Landslides 7(4): 411-423. https://10.1007/s10346-010-0202-3

Chen H, Lin GW, Lu MH, et al. (2011) Effects of topography, lithology, rainfall and earthquake on landslide and sediment discharge in mountain catchments of southeastern Taiwan. Geomorphology 133(3-4): 132-142. https://doi.org/10.1016/j.geomorph.2010.12.031

Chen W, Chai H, Sun X, et al. (2016) A GIS-based comparative study of frequency ratio, statistical index and weights-of-evidence models in landslide susceptibility mapping. Arab J Geosci 9(3): 204. https://doi.org/10.1007/s12517-015-2150-7

Chen W, Pourghasemi HR, Panahi M, et al. (2017) Spatial prediction of landslide susceptibility using an adaptive neuro-fuzzy inference system combined with frequency ratio, generalized additive model, and support vector machine techniques. Geomorphology 297: 69-85. https://doi.org/10.1016/j.geomorph.2017.09.007

Chen W, Wang J, Xie X, et al. (2016) Spatial prediction of landslide susceptibility using integrated frequency ratio with entropy and support vector machines by different kernel functions. Environ Earth Sci 75(20): 1344. https://doi.org/10.1007/s12665-016-6162-8

Choi J, Oh HJ, Lee HJ, et al. (2012) Combining landslide susceptibility maps obtained from frequency ratio, logistic regression, and artificial neural network models using ASTER images and GIS. Eng Geol 124: 12-23. https://doi.org/10.1016/j.enggeo.2011.09.011

Das I, Sahoo S, van Westen C, et al. (2010) Landslide susceptibility assessment using logistic regression and its comparison with a rock mass classification system, along a road section in the northern Himalayas (India). Geomorphology 114(4): 627-637. https://doi.org/10.1016/j.geomorph.2009.09.023

David ER, James LM (1987) Learning Internal Representations by Error Propagation. Parallel Distributed Processing: Explorations in the Microstructure of Cognition: Foundations, MITP: 1.

Derbyshire E, Moniques F, Owen LA (2001) Geomorphological hazards along the Karakoram Highway: Khunjerab Pass to the Gilgit River, Northern Pakistan. Erdkunde 55: 49-71.

Dou J, Bui DT, Yunus AP, et al. (2015) Optimization of causative factors for landslide susceptibility evaluation using remote sensing and GIS data in parts of Niigata, Japan. PloS one 10(7): e0133262. https://doi.org/10.1371/journal.pone.0133262

Dou J, Yamagishi H, Pourghasemi HR, et al. (2015) An integrated artificial neural network model for the landslide susceptibility assessment of Osado Island, Japan. Nat Hazards 78(3): 1749-1776. https://doi.org/10.1007/s11069-015-1799-2

Guzzetti F, Carrara A, Cardinali M, et al. (1999) Landslide hazard evaluation: a review of current techniques and their application in a multi-scale study, Central Italy. Geomorphology 31(1-4): 181-216. https://doi.org/10.1016/S0169-555X(99)00078-1

Guzzetti F, Mondini AC, Cardinali M, et al. (2012) Landslide inventory maps: New tools for an old problem. Earth Sci Rev 112: 42-66. https://doi.org/10.1016/j.earscirev.2012.02.001.

Hewitt K (1999) Quaternary moraines vs catastrophic rock avalanches in the Karakoram Himalaya, northern Pakistan. Quat Res 51(3): 220-237. https://doi.org/10.1006/qres.1999.2033

Hewitt K (2009) Catastrophic rock slope failures and late Quaternary developments in the Nanga Parbat–Haramosh Massif, Upper Indus basin, northern Pakistan. Quat Sci Rev 28(11-12): 1055-1069. https://doi.org/10.1016/j.quascirev.2008.12.019

Hewitt K (2009) Glacially conditioned rock-slope failures and disturbance-regime landscapes, Upper Indus Basin, northern Pakistan. Geological Society, London, Special Publications 320(1): 235-255. https://doi.org/10.1144/SP320.15

Hewitt K (2009) Rock avalanches that travel onto glaciers and related developments, Karakoram Himalaya, Inner Asia. Geomorphology 103(1): 66-79. https://doi.org/10.1016/j.geomorph.2007.10.017

Hung LQ, Van NTH, Duc DM, et al. (2015) Landslide susceptibility mapping by combining the analytical hierarchy process and weighted linear combination methods: a case study in the upper Lo River catchment (Vietnam). Landslides: 1-17. https://doi.org/10.1007/s10346-015-0657-3

Ilia I, Tsangaratos P (2016). Applying weight of evidence method and sensitivity analysis to produce a landslide susceptibility map. Landslides 13(2): 379-397. https://doi.org/10.1007/s10346-015-0576-3

Jones DKC, Brunsden D, Goudie AS (1983) A preliminary geomorphological assessment of part of the Karakoram Highway. Q J Eng Geol Hydrogeol 16: 331-355.

Khan H, Shafique M, Khan MA, et al. (2018) Landslide susceptibility assessment using Frequency Ratio, a case study of northern Pakistan. Egypt J Remote Sens Space Sci. https://doi.org/10.1016/j.ejrs.2018.03.004

Khan H, Shafique M, Khan MA, et al. (2019) Landslide susceptibility assessment using Frequency Ratio, a case study of northern Pakistan. Egypt J Remote Sens Space Sci 22(1): 11-24. https://doi.org/10.1016/j.ejrs.2018.03.004

Khan MA (2000) Tectonics of the Nanga Parbat Syntaxis and the western Himalaya, Geological Society of London.

Kim JC, Lee S, Jung HS, et al. (2018) Landslide susceptibility mapping using random forest and boosted tree models in Pyeong-Chang, Korea. Geocarto Int 33(9): 1000-1015. https://doi.org/10.1080/10106049.2017.1323964

Korup O, Clague JJ, Hermanns RL, et al. (2007) Giant landslides, topography, and erosion. Earth and Planetary Science Letters 261(3–4): 578-589. http://doi.org/10.1016/j.epsl.2007.07.025.

Lee S, Ryu J, Min K, et al. (2001). Development of two artificial neural network methods for landslide susceptibility analysis. IGARSS 2001. Scanning the Present and Resolving the Future. Proceedings. IEEE 2001 International Geoscience and Remote Sensing Symposium (Cat. No.01CH37217).

Lucas AD, Sven F (2017). GIS-Based Logistic Regression for Landslide Susceptibility Analysis in Western Washington State. IJAGR 8(2): 1-19. https://doi.org/10.4018/IJAGR.2017040101

Meng Q, Miao F, Zhen J, et al. (2016) GIS-based landslide susceptibility mapping with logistic regression, analytical hierarchy process, and combined fuzzy and support vector machine methods: a case study from Wolong Giant Panda Natural Reserve, China. B Eng Geol Environ 75(3): 923-944. https://doi.org/10.1007/s10064-015-0786-x

Negnevitsky M (2011) Artificial Intelligence: A Guide to Intelligent Systems. Canada, Pearson Education

Neuhäuser B, Damm B, Terhorst B (2012) GIS-based assessment of landslide susceptibility on the base of the weights-of-evidence model. Landslides 9(4): 511-528.

https://doi.org/10.1007/s10346-011-0305-5

Nohani E, Moharrami M, Sharafi S, et al. (2019) Landslide susceptibility mapping using different GIS-based bivariate models. Water 11(7): 1402.

Owen LA (1988) Wet-sediments deformation in Quaternary and recent sediments in the Kardu Basin, Karakoram Mountains, Pakistan. Glaciotectonics: 123-147.

Ozdemir A, Altural T (2013) A comparative study of frequency ratio, weights of evidence and logistic regression methods for landslide susceptibility mapping: Sultan Mountains, SW Turkey. J Asian Earth Sci 64: 180-197.
https://doi.org/10.1016/j.jseaes.2012.12.014

Park S, Kim J (2019) Landslide susceptibility mapping based on random forest and boosted regression tree models, and a comparison of their performance. Appl Sci 9(5): 942.
https://doi.org/10.3390/app9050942

Pijanowski BC, Brown DG, Shellito BA, et al. (2002) Using neural networks and GIS to forecast land use changes: a land transformation model. Computers, environment and urban systems 26(6): 553-575.
https://doi.org/10.1016/S0198-9715(01)00015-1

Polykretis C, Chalkias C (2018) Comparison and evaluation of landslide susceptibility maps obtained from weight of evidence, logistic regression, and artificial neural network models. Nat hazards 93(1): 249-274.
https://doi.org/10.1007/s11069-018-3299-7

Pradhan B, Lee S (2010) Landslide susceptibility assessment and factor effect analysis: backpropagation artificial neural networks and their comparison with frequency ratio and bivariate logistic regression modelling. Environ Model Softw 25(6): 747-759.
https://doi.org/10.1016/j.envsoft.2009.10.016

Razavizadeh S, Solaimani K, Massironi M, et al. (2017) Mapping landslide susceptibility with frequency ratio, statistical index, and weights of evidence models: a case study in northern Iran. Environ Earth Sci 76(14): 499.
https://doi.org/10.1007/s12665-017-6839-7

Reichenbach P, Rossi M, Malamud BD, et al. (2018). A review of statistically-based landslide susceptibility models. Earth Sci Rev 180: 60-91.
https://doi.org/10.1016/j.earscirev.2018.03.001

Reis S, Yalcin A, Atasoy M, et al. (2012) Remote sensing and GIS-based landslide susceptibility mapping using frequency ratio and analytical hierarchy methods in Rize province (NE Turkey). Environ Earth Sci 66(7): 2063-2073.
https://doi.org/10.1007/s12665-011-1432-y

Riaz MT, Basharat M, Hameed N, et al. (2018) A Data-Driven Approach to Landslide-Susceptibility Mapping in Mountainous Terrain: Case Study from the Northwest Himalayas, Pakistan. Nat Hazards Rev 19(4): 05018007.
https://doi.org/:10.1061/(ASCE)NH.1527-6996.0000302

Rossi M, Guzzetti F, Reichenbach P, et al. (2010) Optimal landslide susceptibility zonation based on multiple forecasts. Geomorphology 114(3): 129-142.
https://doi.org/10.1016/j.geomorph.2009.06.020

Schlögel R, Marchesini I, Alvioli M, et al. (2018) Optimizing landslide susceptibility zonation: Effects of DEM spatial resolution and slope unit delineation on logistic regression models. Geomorphology 301: 10-20.
https://doi.org/10.1016/j.geomorph.2017.10.018

Searle M, Khan MA, Fraser J, et al. (1999) The tectonic evolution of the Kohistan‐Karakoram collision belt along the Karakoram Highway transect, north Pakistan. Tectonics 18(6): 929-949.
https://doi.org/10.1029/1999TC900042

Shafique M, van der Meijde M, Khan MA (2016) A review of the 2005 Kashmir earthquake-induced landslides; from a remote sensing prospective. J Asian Earth Sci 118: 68-80.
http://doi.org/10.1016/j.jseaes.2016.01.002

Shahabi H, Khezri S, Ahmad BB, et al. (2014) Landslide susceptibility mapping at central Zab basin, Iran: A comparison between analytical hierarchy process, frequency ratio and logistic regression models. Catena 115: 55-70.
https://doi.org/10.1016/j.catena.2013.11.014

Umar Z, Pradhan B, Ahmad A, et al. (2014) Earthquake induced landslide susceptibility mapping using an integrated ensemble frequency ratio and logistic regression models in West Sumatera Province, Indonesia. Catena 118: 124-135.
https://doi.org/10.1016/j.catena.2014.02.005

Valencia Ortiz JA, Martínez-Graña AM (2018) A neural network model applied to landslide susceptibility analysis (Capitanejo, Colombia). Geomatics, Nat Hazards and Risk 9(1): 1106-1128.
https://doi.org/10.1080/19475705.2018.1513083

Wang Q, Li W (2017) A GIS-based comparative evaluation of analytical hierarchy process and frequency ratio models for landslide susceptibility mapping. Phys Geogr 38(4): 318-337.
https://doi.org/10.1080/02723646.2017.1294522

Wu Y, Li W, Liu P, et al. (2016) Application of analytic hierarchy process model for landslide susceptibility mapping in the Gangu County, Gansu Province, China. Environ Earth Sci 75(5): 422.
https://doi.org/10.1007/s12665-015-5194-9

Wu Y, Li W, Wang Q, et al. (2016) Landslide susceptibility assessment using frequency ratio, statistical index and certainty factor models for the Gangu County, China. Arab J Geosci 9(2): 1-16.
https://doi.org/10.1007/s12517-015-2112-0

Yalcin A, Reis S, Aydinoglu AC, et al. (2011) A GIS-based comparative study of frequency ratio, analytical hierarchy process, bivariate statistics and logistics regression methods for landslide susceptibility mapping in Trabzon, NE Turkey. Catena 85(3): 274-287.
http://doi.org/10.1016/j.catena.2011.01.014

Yilmaz I (2009) Landslide susceptibility mapping using frequency ratio, logistic regression, artificial neural networks and their comparison: a case study from Kat landslides (Tokat—Turkey). Comput and Geosci 35(6): 1125-1138.
https://doi.org/10.1016/j.cageo.2008.08.007

Youssef AM, Pourghasemi HR, Pourtaghi ZS, et al. (2015) Landslide susceptibility mapping using random forest, boosted regression tree, classification and regression tree, and general linear models and comparison of their performance at Wadi Tayyah Basin, Asir Region, Saudi Arabia. Landslides 13(5): 839-856.
https://doi.org/10.1007/s10346-015-0614-1

Zhou C, Yin K, Cao Y, et al. (2018) Landslide susceptibility modeling applying machine learning methods: A case study from Longju in the Three Gorges Reservoir area, China. Comput and Geosci 112: 23-37.
https://doi.org/10.1016/j.cageo.2017.11.019